

Power Spectrum of a Texture Filled Sky

Jonathan Pearson*

*School of Physics & Astronomy**University of Manchester*

(Dated: August 1, 2008)

We discuss a possible explanation of the observed 5° cold spot in the CMB as being an unwound topological defect known as texture. We briefly discuss the nature of texture. We then discuss numerical simulations of texture populated skies, and numerically find their power spectrum. We then discuss the covariance matrices of texture only skies, finding that textures are non-Gaussian distributed, with zero bispectrum. We also derive the distribution of textures, extending the approximation of Cruz. We derive analytic expressions for the power spectrum of both a single spot & whole sky, and numerically evaluate them; thus providing previously unused computationally trivial methods for finding such spectra.

I. INTRODUCTION

The Cosmic Microwave Background (CMB) is a highly isotropic signature of the very early universe; when the universe was 300,000 years old. The CMB was produced (or, maybe a better word to use is “released”) when the ambient energy of the universe dropped below the ionisation energy of atoms, allowing the otherwise coupled electrons (to the photons) to join nuclei. The photons then became what we call the “CMB”. This era (or, epoch) is what we call, interchangeably, “recombination” or “decoupling”.

The current temperature of the CMB (which was a lot higher, in the past) is $T_0 = 2.725\text{K}$, and is a uniform black body to a very high degree of accuracy. WMAP (Wilkinson Microwave Anisotropy Probe) has been able to map the CMB to incredible accuracy, revealing anisotropies.

The angular spectrum of anisotropies can then be analysed; after subtracting obvious sources such as galactic radiation, the earth motion & known point sources. Such sources are known as the “CMB foreground”.

Now, most anisotropies can be attributed to density perturbations in the early universe; which originated in the inflation epoch, and are generally attributed the role of seeding the universe with large scale structure. It is theorised that in the very early universe (pre-inflation), all elementary particles were indistinguishable, all under a kind of symmetry. However, during inflation, the symmetry was broken, and different particles arose.

Now, misalignments in symmetry breaking give formation of cosmic defects; with different classes of symmetry giving rise to different classes of defects.

A. The “Cold Spot”

When the anisotropies of the CMB are plotted, one finds that there is an “anomalous” cold spot, 5° in ra-

dius, at galactic coordinates having latitude $b = -57^\circ$ and longitude $l = 209^\circ$. This cold spot has no decent explanation as to its origin. Let us clarify this point a little: the CMB (with no texture) is a random distribution, so one can compute the probability of ‘structures’ forming of particular sizes. The probability of a 5° spot forming, under a pure distribution is so small as to be ignored; about 1.85% [1]. Thus, one may invoke the texture theory as a possible explanation of the spot.

When particular groups¹ break into other groups, one finds that topological defects form (which we shall explain a little further, later). A particular class of these defects produces something we call “cosmic texture”, and they are unstable. This defect unwinds after some time (a product of its instability). As they unwind at different times, they appear different sizes: smaller implies further away, larger means closer to us. Now, one of the riding concepts in General Relativity, is that gravitational fields are curvature in space-time, or space-time having a non-trivial metric. Thus, the distorted space around an unwinding texture is actually a time-varying metric.

Any CMB photons passing through this defect will get red- or blue-shifted (depending on where the defect is, relative to the photon). Thus, a hot or cold spot. By way of trivial terminology, we shall use the terms ‘texture’ and ‘spot’ interchangeably.

The magnitude (the observed temperature distortion) of the “spot” is set by the symmetry breaking scale. The size of spots predicted by cosmic textures is in fact consistent with the anomalous cold spot seen in the CMB; as is the number to be found (i.e. only one of such a large size). The number of smaller textures (the limit to “smallness” will be explored, later) is also predicted, but they are generally taken to be smeared out by the CMB photons, thus non-visible to us.

*URL: <http://myweb.tiscali.co.uk/jonathanp>; Electronic address: jap@watering.co.uk

¹ The term ‘group’ is in the context of the mathematical definition of a set of objects, with an associated operation.

B. Introduction to Homotopy Theory

Now, as we shall see later, the topology of the vacuum state (or, generally, the vacuum manifold), determines whether a topological defect forms or not. As two simple examples, consider two potentials: one parabolic, one ‘Mexican hat-like’. The minimum of the parabolic potential (where the minimum of a potential *is* the vacuum state) is a single point. However, the minimum (vacuum state) of the Mexican-hat potential is a circle (in the complex plane). Now, consider a (mathematical) loop “living” in the vacuum manifold. A loop in the parabolic potentials manifold will always be able to be shrunk to infinitesimally small size, whilst remaining in the manifold: the manifold is simply connected. However, consider that a loop moves from the parabolic manifold to the Mexican-hats manifold: if the loop is arranged so that it encompasses the ‘hump’, it cannot be shrunk. That is, shrinking any loop within the vacuum state results in the loop leaving the state. More mathematically speaking, one says that the vacuum manifold \mathcal{M} is disconnected. The type of disconnection then defines what class of defect forms. That a loop used to be able to be shrunk, and now cannot be, defines that a topological defect exists. The example of a loop being shrunk only works in certain dimensions, but it is a useful analogy for others, but must (as with all such analogies) be used with care. The point is that the original group had a set of operations, and that the group changed into another. The original set of operations are no longer valid in the new group.

Consider some space (called a manifold) \mathcal{M} , within which is some point, x . Now, consider that there are some paths which pass through that point x . Now, the paths are said to be “homotopic at x ” if the paths can continuously deform into each other, whilst keeping contact with that point x . As an example, consider that there are three paths f, g, h in \mathcal{M} ; where h passes over some void (i.e. cannot exist within some finite region of space), with f & g not enclosing any “voids”. All three paths pass through the point x . Now, by our previous definition of a path being homotopic, we can see that f & g are homotopic at x , and h is *not* homotopic. That is, one says that f & g are homotopic. We denote such symmetry groups as π_n , where n is the order of the group.

Possibly another way to think about this comes from an analogy in complex integration. If one integrates over a closed path, where the path does not enclose any poles, then one has a zero value for the integral around that path. However, if one integrates over a closed path, with the path enclosing a pole, then one has a non-zero value for the integral; with the value of the integral being the sum over the residues due to that pole.

Basically (and this is without proof, here), a topological defect ‘happens’ when one symmetry group breaks into another. Such as going from a point-manifold, to a circular manifold. The manifolds are the vacuum states of the system. Texture forms from the breaking of π_3 .

Derrick’s theorem states that there are no stable defects above a certain dimension, and texture is the first of such unstable defects.

C. Texture

1. Topological Defects

Let us consider how a texture is produced. As has been previously stated, they are a product of symmetry breaking; we shall consider this now in a little more detail. Now, to begin with, we shall say that there are different types of defect, but they may all be thought about in a similar way. The main difference between the different types of defect, is the dimension of the space in which they are embedded.

Now, a phase transition in a system is governed by the potential a field “feels”. There are two types of potential we shall consider: parabolic & ‘mexican-hat’ type. Let the parabolic potential be denoted $V_1(\phi)$, and the Mexican-hat by $V_2(\phi)$. Infact, let us denote the potential

$$V(\phi) = \frac{1}{\lambda}(\bar{\phi}\phi - \eta^2)^2,$$

so that $\eta = 0$ corresponds to a parabolic, and $\eta \neq 0$ to Mexican hat.

Each has some zero (i.e. a stationary point of the potential) at a position ϕ_0 , so that

$$V_i(\phi_0) = 0.$$

The parabolic potential, centred on zero, gives smooth rolling solutions, which are interesting for inflation. The zero of the parabolic potential occurs at zero. That is

$$V_1(\phi_0) = 0, \quad \phi_0 = 0.$$

In the language of “manifolds”, the vacuum manifold for the parabolic potential is a single point.

The Mexican-hat potential has the interesting property of non-zero vacuum expectation

$$\langle 0 | \phi | 0 \rangle \neq 0.$$

That is, one can see that from the potential, at $\phi = 0$, the potential is non-zero. However, to either side of the position $\phi = 0$ are positions where the potential is zero: $V_2(\phi_0) = 0$; where at the origin

$$V_2(\phi = 0) \neq 0.$$

Any field trapped at the origin $\phi = 0$ (which is an unstable place to be) is tunneled to a minimum ϕ_0 (which is stable). Infact, the Mexican-hat potential V_2 has two minima, symmetrically distributed about the origin. Now, we denote such quantum mechanical tunneling as “transitions”; which are the progenitors of topological

defects. The vacuum manifold for this Mexican-hat potential is a circle.

It should be obvious then that the parabolic potential V_1 is of no use in terms of describing the cosmic topological defects we are considering.

Now, let us state that a field within the symmetry group $O(n)$ (i.e. the group of rotations in an n -dimensional space) is an n -dimensional vector (i.e. has n components), and has the property of non-zero vacuum expectation $\langle 0|\phi|0\rangle \neq 0$.

In 3 spatial dimensions, we can have a number of “classes” of field; fields with different numbers of components; that is, fields belonging to different symmetry groups. In 3D space, the maximum n may be is 4. We merely state this.

So, given some field in some symmetry group, in 3D space, we have 4 possibilities

$$\phi_i \in O(n), \quad i \in [1, n], \quad n \leq 4.$$

That is, a field with either one, two, three or four components. The breaking of different groups give different cosmological topological defects:

- $n = 1$ gives *domain walls*;
- $n = 2$ gives *cosmic strings*;
- $n = 3$ gives *monopoles*;
- $n = 4$ gives *texture*.

Thus, the case interesting to our present discussion, is that of a 4-dimensional vector field ϕ giving rise to textures. So, breaking the rotational symmetry in a plane gives rise to cosmic strings; in a point giving domain walls; etc.

Let us present a simple model of how symmetry breaking works. Consider the attempt at mapping the real plane \mathbb{R}^2 onto the surface of a sphere. Now, this mapping cannot be done, completely: the pole of the sphere will not have come from a point that was originally on the plane. So, consider a closed loop on the plane, where all points within the loop are also within the plane. Then, consider mapping the plane, with the loop, onto the sphere. Now, under certain configurations of the loop, it will then enclose part of the plane which has the missing pole. So, the loop before, could be contracted indefinitely, with all points enclosed by the loop still within the plane. Now, the loop cannot be contracted indefinitely, as there is a point at which the loop will not enclose the space of which it is a part. This is a topological defect.

So, the minima of the potential V form the vacuum manifold \mathcal{M} , which is the non-trivial homotopy group $\pi_3(\mathcal{M}) \neq I$. And this gives rise to texture.

2. Production of a Topological Defect

We are now at a position to bring together many of the ideas we have been developing, to attempt to explain

how a topological defect is formed, and what they are. We shall do so by considering the processes that result in domain walls, but this is entirely analogous.

Consider some parabolic potential, where the minimum of the potential is a single point. Over time, the potential evolves into a Mexican-hat shape. Before any transition occurs, the field sits either at the minimum, or very close to it; this is the state of the field before the potential has changed shape. When the potential changes shape, the field has the ‘choice’ to go to either one of the (new) minima that are either side of the original minimum. Now, the original manifold of vacuum minimum (in the parabolic potential) is not the same as the new vacuum manifold: the two manifolds will belong to different groups. The difference in the groups can be thought of as the difference in the real plane and the surface of a sphere. The difference in manifold dictates what type of defect forms.

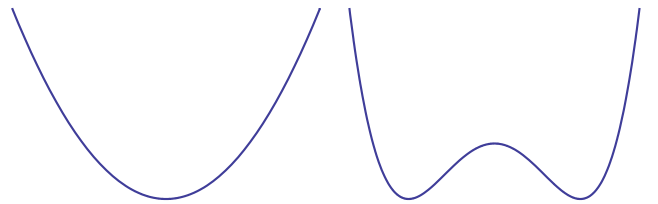


FIG. 1: The parabolic potential (left) and Mexican hat potential (right). During a phase transition, the potential will change, inducing some defect. Going from parabolic to Mexican-hat will induce domain walls as the defect, as the choice to go to the left or right of the maximum is made.

Now, once the field is in its new vacuum manifold, and if the manifold is stable, the field stays there. In the case of the new manifold being the two minima of the Mexican-hat, this will produce two classes of regions of space: one in which the field is at the positive minimum, and one where the field is at the negative. As this happens over a vast causally disconnected region, these portions of space will sit next to each other. If two or more of the same class of space (i.e. two positive pieces) sit next to each other, then this forms a domain. The “walls” between different classes of space will form domain walls.

Now, we said that if the new vacuum manifold is stable, the field will keep its new configuration. But, this need not be the case for all manifolds. The manifold of interest to us, is the manifold which produces texture: the vacuum manifold which the field occupies is unstable. So, once the field has its new vacuum manifold configuration, it will leave that configuration at some point in time. For the case of a four dimensional field, the vacuum manifold is occupied in such a way that it is unstable, so the field leaves the manifold. This is the process of “texture unwinding”. Textures unwind in a way that can be modeled with a time varying metric.

If we consider later results, we will see that an unwinding texture affects a region of space a few hundred Mpc

across, which is a very large region of space.

Another topological defect is a “cosmic string”. These form when the “new” vacuum manifold is a circle. That is, the potential changed from having a point vacuum manifold, to having an irreducible (i.e. unable to shrink back to that point) circular manifold. That the new manifold has a bit missing (the middle section of the circle), gives rise to strings threading through it: cosmic strings.

This theory may be found in [2], [3] and [4]; with the latter reference being one of the first to present textures as a progenitor of cosmic structure. Infact, [5] investigated cosmic strings as providing galaxies with enough mass for the observed rotation curves, with results however suggesting that cosmic strings threading the centre of galaxies are not able to reproduce observed results. Although somewhat off-topic, this is an interesting work, as they attempt to use topological defects in structure formation.

II. METHODS

Here we shall present more technical details on how various procedures are done; and various results attained.

A. Number of Textures

One of the very first problems is to compute the number of spots that will be formed (i.e. the number of texture signatures), that are above a particular scale θ_c . We have that the number of textures, having size θ_c , above some size $\bar{\theta}_c$ is given by [1]

$$N(\theta_c > \bar{\theta}_c) = \frac{4\pi\nu\kappa^3}{3\bar{\theta}_c^2}, \quad (1)$$

which we shall derive later. The size θ_c of the texture is related to the redshift z at which it “unwound” via

$$\theta_c = \frac{2\sqrt{2}\kappa(1+z)}{E(z) \int_0^z \frac{dz'}{E(z')}}, \quad E(z) \equiv \sqrt{\Omega_m(1+z)^3 + \Omega_\Lambda}.$$

The constants ν, κ can be found from [1], with their values given as

$$\nu = 2, \quad \kappa = 0.1.$$

We take the relative densities of matter & dark energy to be

$$\Omega_m = 0.26, \quad \Omega_\Lambda = 0.74.$$

We shall now discuss how to find the number of textures in the sky, between some upper and lower bounds. We shall then discuss how to find the number of textures of a particular size; that is, how many textures are in the sky, of arbitrary size θ_c .

1. Number of Spots: Method

So then, from the number of spots above a given size, we can compute the number of spots of a given size. Consider the integral

$$N = \int_{n_1}^{n_2} dN.$$

This will find the number of N 's in the range $n_1 \leq N \leq n_2$. Then, consider multiplying & dividing by $d\theta_c$, and taking the lower limit to some value $\bar{\theta}_c$ and the upper limit to infinity. Then, this will give the number of spots, above the size $\bar{\theta}_c$

$$N(\theta_c > \bar{\theta}_c) = \int_{\bar{\theta}_c}^{\infty} \frac{dN}{d\theta_c} d\theta_c. \quad (2)$$

Now, we know the answer to this, (1). So, its not too hard to see that the differential is quite straightforward, in being²

$$\frac{dN}{d\theta_c} = \frac{8\pi\nu\kappa^3}{3\theta_c^3}. \quad (3)$$

This can be thought of as a “density of states” type-expression. So, dividing out, trivially

$$dN = \frac{8\pi\nu\kappa^3}{3\theta_c^3} d\theta_c.$$

Thus giving an expression for the number of spots in a size range $\theta_c \rightarrow \theta_c + d\theta_c$.

Now, consider the expression

$$r = \frac{\int_{\theta_c^{\min}}^{\theta_c} \frac{dN}{d\theta_c} d\theta_c}{N_{\text{tot}}}, \quad (4)$$

where we have the total number of spots N_{tot} in a range $\theta_c^{\min} \rightarrow \theta_c^{\max}$

$$N_{\text{tot}} = \int_{\theta_c^{\min}}^{\theta_c^{\max}} \frac{dN}{d\theta_c} d\theta_c.$$

This easily evaluates to, using (3),

$$N_{\text{tot}} = -\frac{4\pi\nu\kappa^3}{3} \left[\frac{1}{(\theta_c^{\max})^2} - \frac{1}{(\theta_c^{\min})^2} \right].$$

Now, consider the integral in the numerator of (4): it is the number of spots, between some minimum and θ_c . So, dividing that number by the total number of spots will always give a number between zero and unity. Thus,

² We use Leibniz' rule for integration, which leaves this quantity positive, as opposed to negative.

$r \in [0, 1]$. So, using the density of states expression, (3), in (4), we see that

$$r = \frac{\frac{1}{\theta_c^2} - \frac{1}{(\theta_c^{\min})^2}}{\frac{1}{(\theta_c^{\max})^2} - \frac{1}{(\theta_c^{\min})^2}}$$

is easily attained. This is readily inverted, to make θ_c the subject. So, the point of this is that given a number r , where $r \in [0, 1]$, we can compute some ‘‘associated’’ spot size θ_c .

We must choose the minimum θ_c^{\min} & maximum θ_c^{\max} spot sizes both small & big, respectively; thus, we choose

$$\theta_c^{\min} \approx 10 \text{ arc mins} \quad \theta_c^{\max} \approx 30^\circ.$$

The written program consisted of a random number generator, to provide some r , to be used to compute some θ_c . This generation then conformed to the distribution expected.

It is worth noting that the maximum size of a spot predicted, by the approximate method, is 5° ; and that there is only one of that size (on average). There are more predicted, of lower size.

Thus, statistically, if we run this for a very large number of systems, the approximate r -method will average-out to the exact value. This is a very important technique that will be extensively used. We say that we generate many realisations, and average.

2. Number of Spots: Derivation

We shall now derive the result (1) quoted above.

From Cruz, we have that the number of textures, above size θ_c which unwound at conformal time τ_z , is given by considering the number of unwinding textures in a volume, where the volume extends back in time until the first texture of interest unwound. That is, we can compute the number of textures above a given size θ_c , where that size is due to a texture unwinding at conformal time τ_z , via

$$N_{\text{spot}} = \int_{\tau_z}^{\tau_0} d\tau \frac{dn}{d\tau} 4\pi(\tau_0 - \tau)^2 \int_{\theta_c(\tau_0 - \tau)}^{\kappa\tau} 2dr, \quad (5)$$

where τ_0 is the current conformal time; and the factor of 2 is due to there being both hot & cold spots. This integral may be found in [2]. The number of textures unwinding, per unit comoving volume, is given by

$$\frac{dn}{d\tau} = \frac{\nu}{\tau^4}.$$

Now, let us look at the limits on the dr -integral in (5). We obviously must have that the upper limit is greater than the lower. Thus

$$\kappa\tau > \theta_c(\tau_0 - \tau).$$

And therefore we must have, everywhere

$$\tau > \frac{\theta_c\tau_0}{\kappa + \theta_c}. \quad (6)$$

Now, we must impose a restriction: texture that we see ‘‘now’’ are only those which have unwound since recombination, which occurred at some time τ_{rec} . So, we also therefore have $\tau > \tau_{\text{rec}}$; hence, we see that we must have

$$\frac{\theta_c\tau_0}{\kappa + \theta_c} > \tau_{\text{rec}}.$$

Rearranging, we get a fundamental lower limit on the spot size θ_c

$$\theta_c > \frac{\tau_{\text{rec}}\kappa}{\tau_0 - \tau_{\text{rec}}} \equiv \theta_c^{\min}, \quad (7)$$

which we come back to later. So then, using the lower limit (6) in (5), we have

$$N_{\text{spot}} = \int_{\frac{\theta_c\tau_0}{\kappa + \theta_c}}^{\tau_0} d\tau \frac{dn}{d\tau} 4\pi(\tau_0 - \tau)^2 \int_{\theta_c(\tau_0 - \tau)}^{\kappa\tau} 2dr. \quad (8)$$

Thus, integrating and therefore the number of spots, above some size θ_c

$$N_{\text{spot}} = 8\pi\nu \left\{ \frac{\kappa^3}{6\theta_c^2} + (\kappa + \theta_c) \ln \left(\frac{\kappa + \theta_c}{\theta_c} \right) + \frac{7\kappa^2}{2\theta_c} + 5\kappa \right\}. \quad (9)$$

We see that we can recover Cruz’ result by ignoring all but the first term;

$$N_{\text{spot}} \approx \frac{8\pi\nu\kappa^3}{6\theta_c^2} = \frac{4\pi\nu\kappa^3}{3\theta_c^2}.$$

Where this is the result quoted in Cruz.

Infact, through a little more analysis, one finds that the logarithmic term does not appreciably affect the number of spots.

We present a comparison of Cruz’ distribution, and the derived distribution, in Fig (2). The functions that we plot are

$$\Theta_1 \equiv 8\pi\nu \frac{\kappa^3}{6\theta_c^2}, \quad (10a)$$

$$\Theta_2 \equiv 8\pi\nu \left(\frac{7\kappa^2}{2\theta_c} + 5\kappa \right) + \Theta_1, \quad (10b)$$

where we plot dN , as before. From the plot, we see that we cannot ignore the correction term.

So, from (9), we can derive the new density of states (ignoring the log term)

$$\frac{dN}{d\theta_c} = 8\pi\nu \left(\frac{\kappa^3}{3\theta_c^3} + \frac{7\kappa^2}{2\theta_c^2} \right). \quad (11)$$

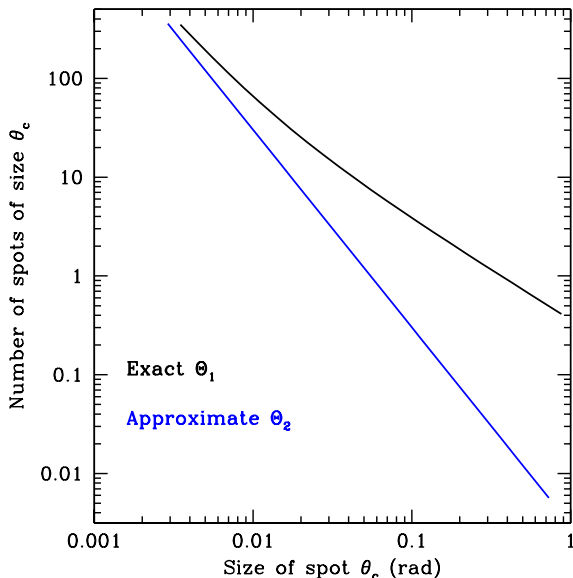


FIG. 2: Testing the approximation used in Cruz. Functions Θ_i are defined by (10)

We shall refer to (3) as Cruz' distribution (or, the approximate), and (11) as the derived distribution; with results quoting which is used.

Let us recall the formalism behind (4). So again, we may provide some random number $r \in [0, 1]$, and we will thus find an associated θ_c ; see Fig (3) for the graphical solution.

It is fairly easy to compute the total number of textures, between $\theta_c^{\min} = 0.003$ and $\theta_c^{\max} = 0.5$. We find that using Cruz' approximate distribution, we have ≈ 900 , and using the exact derived distribution ≈ 1500 textures per sky.

3. Minimum Spot Size

Let us now compute the (ideal) minimum spot size. We have derived an expression, in (7)

$$\theta_c^{\min} = \frac{\tau_{\text{rec}} \kappa}{\tau_0 - \tau_{\text{rec}}}, \quad (12)$$

where $\tau_0, \tau_{\text{rec}}$ are the conformal times at the observation point (i.e. now) and at recombination. Let us consider how to compute conformal times. Let us state that the derivative of the scale factor, with respect to conformal time is

$$\dot{a} = \frac{da}{d\tau}.$$

And therefore, we easily see that

$$\int_0^{\tau_i} d\tau = \int_0^{a_i} \frac{da}{\dot{a}},$$

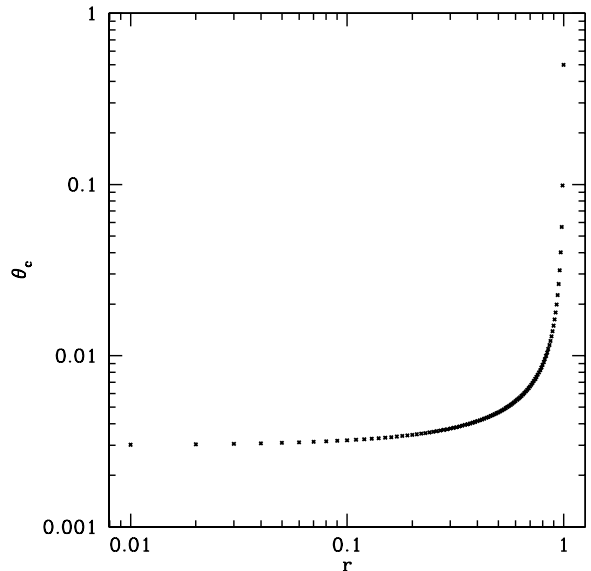


FIG. 3: Given a random number r , one can then find the associated spot size θ_c . This is the solution using the derived equation (11).

where τ_i, a_i are the conformal time, scale factor, at the time of interest. Now, we also have a relation between scale factor and the Hubble parameter: $H = \dot{a}/a$. Via fairly simple arguments, we can derive

$$\dot{a} = H_0 \sqrt{\Omega_r + \Omega_m a + \Omega_\Lambda a^4},$$

where H_0 is the present value of the Hubble parameter $\approx 2 \times 10^{-18} \text{s}$. This leads us to be able to write

$$\int_0^{\tau_i} d\tau = \frac{1}{H_0} \int_0^{a_i} \frac{da}{\sqrt{\Omega_r + \Omega_m a + \Omega_\Lambda a^4}}.$$

This must be numerically integrated. So, using $\Omega_r = 0, \Omega_m = 0.26, \Omega_\Lambda = 0.74$ we get the following conformal times relating to scale factors:

$$\begin{aligned} a_0 = 1 &\quad \Rightarrow \quad \tau_0 = 5.5 \times 10^{10} \text{yrs.} \\ a_{\text{rec}} = 9 \times 10^{-4} &\quad \Rightarrow \quad \tau_{\text{rec}} = 1.86 \times 10^9 \text{yrs.} \end{aligned}$$

Where we have derived the recombination scale factor a_{rec} by noting that $a_{\text{rec}} = T_0/T_{\text{rec}}$, taking $T_0 = 2.725 \text{K}$ and $k_B T_{\text{rec}} = 0.25 \text{eV}$. Thus using these numbers (converting the conformal times into seconds) results in, via (12)

$$\theta_c^{\min} = 3.48 \times 10^{-3} \text{rad.}$$

And therefore we have computed the fundamentally minimum spot size.

4. Temperature Distortion

From Cruz's paper [1] (originally derived in [6] and [7]), we have an expression for the temperature distortion

around a spot, of given observed size θ_c

$$\frac{\Delta T}{T}(\theta) = \pm \frac{\epsilon}{\sqrt{1 + 4 \left(\frac{\theta}{\theta_c}\right)^2}}, \quad (13)$$

where the magnitude of the distortion, ϵ , is given (from Cruz) by

$$\epsilon = 4 \times 10^{-5}.$$

This number is actually found from $\epsilon = 8\pi^2 G \phi_0^2$, where ϕ_0 is the symmetry breaking energy scale. That is, we can match the observed magnitude of temperature distortion with a value of ϕ_0 ; thus constraining the value. This number is of great significance in particle physics. In the derivation of (13) (i.e. in [6]), one assumes that $\dot{a} = 0$. It is thought to be this assumption that gives the distribution its logarithmic behavior at large θ . We have attempted to re-derive without this assumption, but lack of time has prevented a useful result.

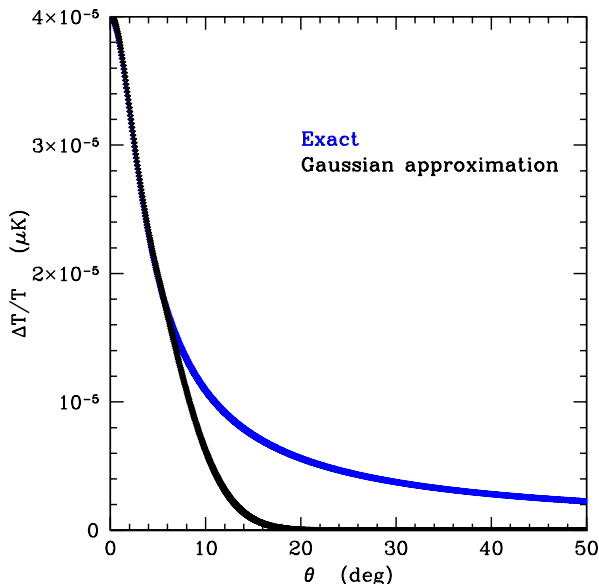


FIG. 4: The exact temperature distortion (13) for a typical texture; and the Gaussian approximation (15) at half-max. The temperature difference $\Delta T/T$ is shown, for an angle θ away from the centre. This is a texture at $z = 20$.

We shall approximate the temperature distortion, in the same way as in Cruz. We shall approximate the temperature distortion, beyond its half maximum, by a Gaussian; this is in attempt at picking up some of the power that is in the “tail” of the distortion. That is, the exact distortion actually goes like $1/\theta^2$, hence one will go round the sky more than once to pick up all distortion. Consider that the temperature distortion is defined thus

$$f(\theta) = \pm \frac{\epsilon}{\sqrt{1 + 4 \left(\frac{\theta}{\theta_c}\right)^2}},$$

and that we have some Gaussian:

$$g(\theta) = A e^{-\theta^2/2\sigma^2}.$$

So, at the position of half maximum, we have

$$f(\theta_{HM}) = \frac{f(0)}{2}.$$

And so, we can fairly easily derive the position of half maximum, θ_{HM} , for a given spot size θ_c

$$\theta_{HM} = \frac{\theta_c \sqrt{3}}{2}.$$

So, we make the value & derivative of f the same as g , at θ_{HM}

$$f(\theta_{HM}) = g(\theta_{HM}), \quad f'(\theta_{HM}) = g'(\theta_{HM}).$$

And thus, we have two equations, from which we can solve for the two unknowns: the amplitude A & mean σ .

So, from $f(\theta_{HM}) = g(\theta_{HM})$, we have

$$A = \frac{\epsilon}{2} e^{3\theta_c^2/8\sigma^2}. \quad (14)$$

We can compute the derivatives

$$\begin{aligned} f'(\theta_{HM}) &= -\frac{\epsilon\sqrt{3}}{4\theta_c}, \\ g'(\theta_{HM}) &= -\frac{A\theta_c\sqrt{3}}{2\sigma^2} e^{-3\theta_c^2/8\sigma^2}, \end{aligned}$$

and by matching the derivatives $f'(\theta_{HM}) = g'(\theta_{HM})$, we obtain that $\sigma = \theta_c$. Then, using this in (14) results in a complete Gaussian fit to the temperature distortion, for distances beyond half maximum

$$g(\theta) = A e^{-\theta^2/2\sigma^2}, \quad A = \frac{\epsilon}{2} e^{3/8}, \quad \sigma = \theta_c, \quad \theta \geq \frac{\theta_c}{2} \sqrt{3}. \quad (15)$$

In a similar way, we can derive a general expression for the Gaussian which fits onto the temperature distortion, once the distortion has passed a fraction

$$f(\theta_n) = \frac{f(0)}{n}.$$

Thus, we find

$$A = \frac{\epsilon}{n} e^{(n^2-1)/(2n^2)}, \quad \sigma = \frac{n\theta_c}{2}, \quad \theta \geq \frac{\theta_c}{2} \sqrt{n^2-1}. \quad (16)$$

So that (15) corresponds to $n = 2$.

B. CMB Realisation

Now, to discuss the CMB realisation concept, we must first discuss the way in which the CMB is decomposed.

1. Decomposition of the CMB

Decomposition of a function into spherical harmonics is entirely analogous to decomposing a function using Fourier series: one does so by considering the amplitude of a particular mode (or harmonics) that the function ‘uses’. A common use of Fourier decomposition is in the vibration of a string. If the string is vibrating at a pure frequency, then the decomposition will only have one term (i.e. a single harmonic). However, the motion of the string will be (in general) a sum over many harmonics. As a very non-rigorous way to think of this, consider money: coins come in denominations of 1p, 2p, 5p, 10p, 20p etc. So, consider that something costs 3p: to pay for it one must use coins of two denominations (or, three of one; the case of which we shall ignore). However, for something costing 20p, one may use a single 20p piece. Purchasing items is done by decomposing the total cost into particular modes, or denominations, of coins. Infact, an interesting sideline that this case highlights is that of “degeneracy”: as we saw, there is more than one way of making 3p: either 1p & 2p, or 3 1p pieces. There is generally more than one way of arranging the modes to give the same end result. Consider that a mode (i.e. a denomination of coin) is denoted C_i ; and that the number of a particular coin is some number a_i . Then to make a total amount T , we must form the sum

$$T = \sum_i a_i C_i; \quad C_i = \{1p, 2p, 5p, 10p, 20p\}.$$

For example, if $T = 67p$, we can make this total amount by

$$T = 67p = (3 \times 20p) + (1 \times 5p) + (1 \times 2p).$$

Here, we see that the set of coefficients is $a_i = \{3, 1, 1\}$, and we only took the modes $C_i = \{20p, 5p, 2p\}$. Also note that the amount 67p itself isn’t a denomination, but it may be formed from a sum of modes. This should now be clear how a decomposition works. Let us get back on topic.

We may imagine that the CMB is on a sphere, centred on us; and we may thus decompose the anisotropies of the CMB in terms of spherical harmonics, using some coefficient $a_{\ell m}$ to denote the amplitude of each harmonic used

$$\frac{\Delta T}{T}(\theta, \phi) = \sum_{\ell=2}^{\infty} \sum_{m=-\ell}^{\ell} a_{\ell m} Y_{\ell m}(\theta, \phi).$$

Notice that we have excluded the monopole & dipole modes from the decomposition: they are not of primordial origin. The monopole is just the uniform background, and the dipole the earths motion relative to the CMB.

The constants $a_{\ell m}$ are in general complex; with the exception of $m = 0$, in which case we have axial symmetry, and $a_{\ell 0}$ is real;

$$a_{\ell m} \in \mathbb{C} \quad \forall m \neq 0, \quad a_{\ell 0} \in \mathbb{R}.$$

Now, we relate spherical harmonics to the associated Legendre polynomials via

$$Y_{\ell m}(\theta, \phi) = \sqrt{\frac{2\ell+1}{4\pi} \frac{(\ell-m)!}{(\ell+m)!}} e^{im\phi} P_{\ell}^m(\cos\theta), \quad (17)$$

where spherical harmonics are normalised

$$\int Y_{\ell' m'}^*(\theta, \phi) Y_{\ell m}(\theta, \phi) d\Omega = \delta_{\ell\ell'} \delta_{mm'};$$

and therefore, by the orthonormality relation, we can find the coefficients $a_{\ell m}$ via

$$a_{\ell m} = \int \frac{\Delta T}{T}(\theta, \phi) Y_{\ell m}^*(\theta, \phi) d\Omega.$$

Now, one can define the angular correlation function $C(\theta)$,

$$C(\theta) \equiv \left\langle \frac{\Delta T}{T} \right\rangle^2 = \frac{1}{4\pi} \sum_{\ell} \sum_m |a_{\ell m}|^2 P_{\ell}(\cos\theta),$$

which, under a definition of C_{ℓ} , which we will come to, gives

$$C(\theta) = \frac{1}{4\pi} \sum_{\ell} (2\ell+1) C_{\ell} P_{\ell}(\cos\theta),$$

where we have defined

$$C_{\ell} \equiv \frac{1}{2\ell+1} \sum_m |a_{\ell m}|^2.$$

The above sums over m run from $m = -\ell \rightarrow +\ell$, over all available ℓ values.

So, given some set of constants $a_{\ell m}$, one may construct an anisotropic “sky”. Let us briefly discuss how this was achieved.

2. Computing $a_{\ell m}$

Here, we detail how to create a Gaussian realisation of the CMB. We do so by computing a random set of $a_{\ell m}$, and use those in our analysis. This method will give a completely isotropic sky, over many realisations.

Now, from $\ell = 2$ to $\ell = \ell_{max}$; and for $m \in [-\ell, \ell]$; we must compute some random numbers to use as the real and imaginary parts of the constant $a_{\ell m}$,

$$a_{\ell m} \equiv \zeta_1 + i\zeta_2, \quad \zeta_j \in \mathbb{R} : j = 1, 2.$$

where, obviously, i is the complex number $i = \sqrt{-1}$. To do this, we first compute two random, uniform, deviates x_j (say). We then use a procedure to transfer the uniform x_j to normal deviates y_j ;

$$y_1 = \sqrt{-2 \ln x_1} \cos(2\pi x_2), \quad y_2 = \sqrt{-2 \ln x_1} \sin(2\pi x_2).$$

The theory behind this “change of random numbers” may be found in [8]. These normal “random deviates” can then be used to compute the ζ_j ,

$$\zeta_j \equiv \sqrt{\frac{C_\ell}{2}} y_j, \quad j = 1, 2.$$

We shall soon discuss the constant C_ℓ . Notice that as these are normalised deviates

$$\zeta_1^2 + \zeta_2^2 = \frac{C_\ell}{2} y_1^2 + \frac{C_\ell}{2} y_2^2 = C_\ell. \quad (18)$$

Thus, we can compute a random set of $a_{\ell m}$

$$a_{\ell m} = \zeta_1 + i\zeta_2, \quad \forall \ell \in [2, \ell_{max}], |m| \leq \ell.$$

The real numbers ζ_j are unique (up to the random generator) for every value of ℓ, m ; we leave off the possibly illuminating superscripts $\zeta_j^{\ell m}$ which would denote this, for clarity in other respects. Notice that the real requirement for the $m = 0$ case is in fact the requirement that $\zeta_2 = 0$ for all $m = 0$, and any ℓ .

Thus, we see that we are limiting the resolution of the decomposition by the maximum mode ℓ_{max} , which we must impose for any numerical calculation. This number is always quoted with a result.

3. The role of C_ℓ

Now, we shall immediately start by distinguishing the “approximate” C_ℓ with the “exact” \hat{C}_ℓ ; one without a hat, one with.

The exact \hat{C}_ℓ is defined by

$$\hat{C}_\ell \equiv \frac{1}{2\ell + 1} \sum_{m=-\ell}^{\ell} |a_{\ell m}|^2.$$

So, this, under the notation that $a_{\ell m} = \zeta_1^{\ell m} + i\zeta_2^{\ell m}$, is

$$\hat{C}_\ell = \frac{1}{2\ell + 1} \sum_m |\zeta_1^{\ell m}|^2 + |\zeta_2^{\ell m}|^2.$$

Thus, the expectation value $\langle \hat{C}_\ell \rangle$

$$\langle \hat{C}_\ell \rangle = \frac{1}{2\ell + 1} \sum_m \left(\frac{C_\ell}{2} + \frac{C_\ell}{2} \right) = \frac{C_\ell}{2\ell + 1} \sum_m 1 = C_\ell,$$

where we have made use of the normalised deviates from (18). We have also used the standard result that there are $2\ell + 1$ values of m for a given ℓ . So we see that an average of C_ℓ will give the exact \hat{C}_ℓ , where an average taken over an infinite sample will give the exactly correct result. Again, as we said previously, we say that we take an average over realisations.

Now, the expression for the exact \hat{C}_ℓ can be easily found from

$$\left(\frac{\Delta T}{T} \right)^2 = \frac{\ell(\ell + 1)}{2\pi} \hat{C}_\ell.$$

This result comes from a standard method in decomposing the anisotropies.

So again, we have a method for computing approximate anisotropies, when averaging over many systems (i.e. over many “realisations”) we will average out to the exact value.

We tend to plot ℓ against $C_\ell \frac{\ell(\ell+1)}{2\pi}$. The exact will just be horizontal line, of height the temperature difference; and the approximate will be scattered around the exact value (for an isotropic sky). Again, as was previously stated, if many of the approximate values of C_ℓ are computed, for the same ℓ , the average will be the exact values \hat{C}_ℓ .

Plotting ℓ against $C_\ell \ell(\ell + 1)/2\pi$ constitutes plotting a *power spectrum*. We also find that Gaussian random variables conform to

$$\frac{\sigma_{C_\ell}}{C_\ell} = \sqrt{\frac{2}{2\ell + 1}}, \quad (19)$$

where σ_{C_ℓ} is the standard deviation on C_ℓ . This will hold exactly for an infinite number of realisations, but for a finite amount will oscillate about the exact value; and non-Gaussian distributes lying off the line appreciably.

C. Power Spectra

Now, given a set of $a_{\ell m}$ ’s, we can compute the coefficient C_ℓ as we have seen,

$$C_\ell = \frac{1}{2\ell + 1} \sum_{m=-\ell}^{+\ell} |a_{\ell m}|^2.$$

We get the $a_{\ell m}$ from a decomposition of (any) pattern (or distribution) on a sphere, into spherical harmonics. So, given a distribution (for example, the temperature fluctuations of randomly placed texture-spots), one may decompose that pattern into spherical harmonics; where, along the way, one will derive the $a_{\ell m}$, and thus one may plot the power spectrum via the C_ℓ .

The way this is actually done, was using a subroutine from the Fortran90 distribution of JPL’s HEALPix software. The subroutine, *map2alm*, takes some (one-dimensional) array³ which represents the map *map(i)*, and decomposes the map into spherical harmonics, outputting the coefficients $a_{\ell m}$. Obviously, this is only within pre-defined bounds; such as the maximum decomposition mode ℓ_{max} and number of pixels of the map (the pixel number is n_{pix} , but we usually work in terms of N_{side} , where $n_{pix} = 12N_{side}^2$). A typical map has

³ An *array*, for those unaware of such a phrase, is the programmers-language for a vector. In the same way as one has an n -dimensional vector \mathbf{v} having n -components, where a component is represented as v_i , and that element can be any number; so an array element *map(i)* represents any number.

$N_{side} = 128$ (and thus $\approx 2 \times 10^5$ pixels). All results in this paper use the higher resolution $N_{side} = 256$.

1. The Sky as a Map

Let us briefly discuss how HEALPix ‘views’ (and thus, how we must view) the sky.

We take some one-dimensional array, *map*, having the same number of elements as pixels (i.e. resolution) of the sky. So, we initially think of the entire sky in terms of pixels, where each pixel represents some position (θ, ϕ) . So, given a position i inside the array (i.e. which component of the vector), we may discover what θ, ϕ it represents, via the HEALPix routine *pix2ang*. It takes, as its argument, some integer i , which is just the element of the array, and outputs the spherical angles θ, ϕ corresponding to that i .

As was previously stated, we use a resolution (i.e. number of pixels) of the order 10^5 . Thus, we have an array with 10^5 elements.

Once we have found the position on the sky (via *pix2ang*), one may then think about the value of the map at that point: the temperature of the sky, at that point. For (as an utterly arbitrary) example, consider the statement

$$map(87) = (\theta = 9^\circ, \phi = 78^\circ) = 5K.$$

So, we see that the temperature of the sky, at coordinates $(9^\circ, 78^\circ)$ is 5K. And this position (i.e combination of θ, ϕ) is unique to the 87th-element of the array *map*.

D. Populating the Sky with Texture

Now, the problem at hand is to distribute at random positions on the sky, a whole range of texture ‘spots’, where a spot of a particular size θ_c has a well defined temperature profile

$$\frac{\Delta T}{T}(\vartheta) = \pm \frac{\epsilon}{\sqrt{1 + 4 \left(\frac{\vartheta}{\theta_c}\right)^2}}.$$

Now, one will notice a change in symbol from (13): the ‘ θ ’ in (13) represented the distance from the centre of the spot. So, we use the symbol ϑ to denote the distance from the centre of the spot, to distinguish from the coordinate θ . Also, its worth noting that the sign of the distortion is random. Now, as per previous discussion, we have seen that there is a well defined number of spots, of a particular size. The sizes of spots, θ_c , is defined within some range

$$\theta_c^{\min} \leq \theta_c \leq \theta_c^{\max}.$$

Recall that the number of spots above θ_c is $\propto 1/\theta_c^3$; thus, for very small sizes, there are very large number

of spots. This large number makes computation very lengthy. Thus, we must truncate at some lower bound, higher than the fundamental minimum. The dependence of various parameter on this bound is discussed later.

So, computationally, let us discuss how to populate a sky with textures only (as opposed to texture & ‘CMB’).

We first create some array, which is our map, where the value of each element of the array is the temperature of the sky, at that position (initially set to zero, everywhere). The next thing to compute is the total number of spots, between a lower bound (θ_c^{\min}), and higher bound (θ_c^{\max}), N_{tot} (this has already been discussed). Once this has been established, one must then compute the number of spots, of each size (where the interval between sizes must be discretised in some way). For our current discussion, suppose that there is a number N_i of spots of size θ_c^i .

Once N_i has been established, one must then find some random position on the sky to place the centre of the spot. Suppose that we find some random positions θ_p^i, ϕ_p^i as the centre of that spot. This position on the sky must then be converted into a position on the array. So, we have the position of the centre of a single spot. What one must then compute is the temperature everywhere on the sky, due to that spot. So, one must then look at every element of the array (i.e. pixel), compute the distance from that point to the spot, and compute the temperature distortion at that point due to the spot. Suppose that the pixel has position θ_t, ϕ_t , and that the spot is centred on θ_p^i, ϕ_p^i . Then, one computes the distance from the spot to the pixel, using the spherical line element

$$\vartheta^2 = d\theta^2 + \sin^2 \theta_t d\phi^2; \quad d\alpha = \alpha_p^i - \alpha_t, \quad \alpha \equiv \{\theta, \phi\}.$$

Given this distance, one can then compute the temperature at that point. The procedure must then be done again, for every element of the map-array (and therefore for every point on the sky), for that single spot. Thus, we will have the temperature distortion on the sky, due to a single texture.

This entire procedure must then be repeated for every spot of every size. Thus, as one may imagine, this is a very processor-heavy procedure! Thus, this procedure will have created a single map of a sky of textures.

1. Texture Power Spectrum

Once a map has been simulated, one then decomposes into $a_{\ell m}$ ’s, using HEALPix, and thus find the power spectrum. In practice, the power spectrum is the average over many realisations. See Fig (13) for a visualisation of a texture-filled sky.

We display the power spectra for a simulated texture only sky, in Fig (5). See Fig (6) for a brief analysis of the power spectrum with different Gaussian fits. Fig (8) shows the power spectrum, using the derived distribution (11) & Cruz’ (3). Although not printed here, we have

plotted (19), and we find that all points lie above the line, thus giving weight to textures not being Gaussian.

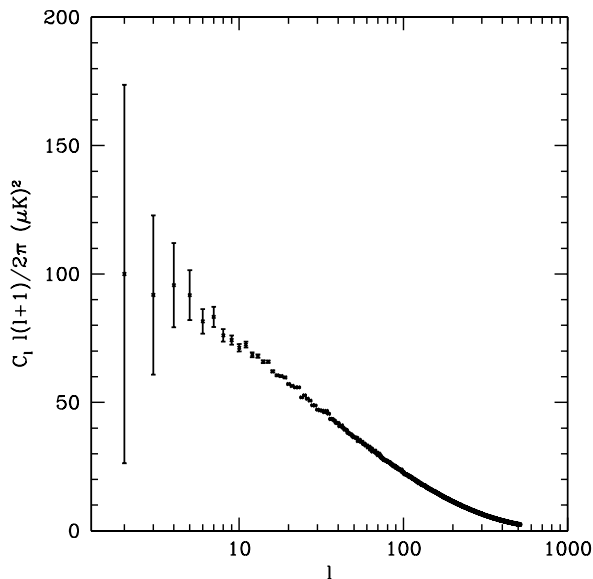


FIG. 5: The texture power spectrum. Using 250 realisations, $\ell_{max} = 512$, $\theta_c^{max} = 0.52$, $\theta_c^{min} = 0.003$; as well as the exact temperature distortion & Cruz' distribution.

E. Analytical Power Spectrum

Let us derive the single spot power spectrum, from first principles.

We know that the $a_{\ell m}$ may be found from

$$a_{\ell m} = \int d\Omega f(\theta, \phi) Y_{\ell m}^*(\theta, \phi),$$

but considering that our function

$$f(\theta, \theta_c) \equiv \frac{\epsilon}{\sqrt{1 + 4 \left(\frac{\theta}{\theta_c}\right)^2}}$$

is a function of θ (and θ_c ; but it is not a spatial coordinate) only, we use the relation between spherical harmonics and the associated Legendre polynomials (17), leaving us with

$$a_{\ell m}(\theta_c) = \sqrt{\frac{2\ell + 1}{4\pi} \frac{(\ell - m)!}{(\ell + m)!}} \times \int_0^\pi \sin \theta d\theta f(\theta, \theta_c) P_\ell^m(\cos \theta) \int_0^{2\pi} e^{im\phi} d\phi,$$

that is,

$$a_{\ell m}(\theta_c) = 2\pi \delta_{m0} \sqrt{\frac{2\ell + 1}{4\pi}} \int_0^\pi \sin \theta f(\theta, \theta_c) P_\ell(\cos \theta) d\theta.$$

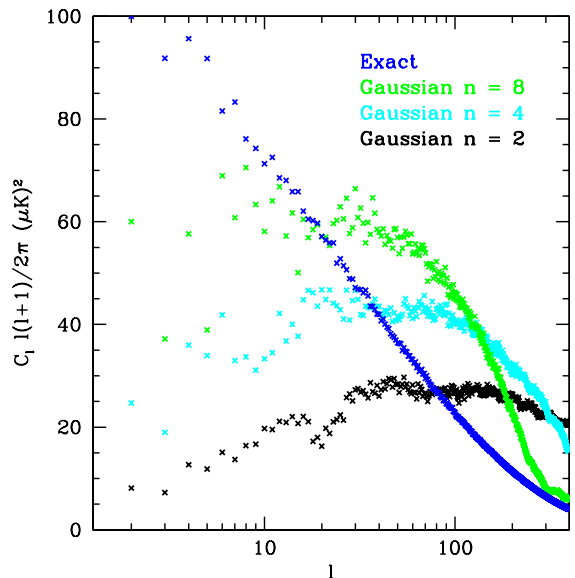


FIG. 6: Texture only power spectra. Numerical analysis of the dependance of the power spectra on Gaussian temperature fit. This plot uses the exact temperature distortion, and three Gaussian approximations: at 8th-max, quarter max, and at half-max; corresponding to $n = 8, 4, 2$. The exact power spectrum is from 200 realisations; the Gaussians from 20. Using Cruz' distribution.

Now, the power spectrum coefficient is defined as

$$C_\ell = \frac{1}{2\ell + 1} \sum_m |a_{\ell m}|^2,$$

which is just

$$C_\ell(\theta_c) = \pi \left[\int_0^\pi \sin \theta f(\theta, \theta_c) P_\ell(\cos \theta) d\theta \right]^2.$$

So, putting in our function, results in

$$C_\ell(\theta_c) = \pi \left[\int_0^\pi \frac{\epsilon \sin \theta P_\ell(\cos \theta)}{\sqrt{1 + 4 \left(\frac{\theta}{\theta_c}\right)^2}} d\theta \right]^2. \quad (20)$$

If we use the Bessel function approximation

$$P_\ell(\cos \theta) \sin \theta \approx J_0([\ell + 0.5]\theta)\theta, \quad (21)$$

whilst taking the limit to ∞ ,

$$C_\ell(\theta_c) = \pi \left[\int_0^\infty \frac{\epsilon J_0([\ell + 0.5]\theta)\theta}{\sqrt{1 + 4 \left(\frac{\theta}{\theta_c}\right)^2}} d\theta \right]^2. \quad (22)$$

And therefore, we have computed the power spectrum coefficient, for a single texture, size θ_c .

1. Full Distribution Power Spectrum

Following from the single spot power spectrum (20), it is semi-trivial to extend the analytic expression for the power spectrum, to a full distribution of textures. Rather than choosing some θ_c , we allow an integral to sweep over all possible values, weighted by the density of states. That is, for a full distribution,

$$C_\ell = \pi \int_{\theta_c^{\min}}^{\theta_c^{\max}} \frac{dN}{d\theta_c} d\theta_c \left[\int_0^\pi \frac{\epsilon \sin \theta P_\ell(\cos \theta)}{\sqrt{1 + 4 \left(\frac{\theta}{\theta_c}\right)^2}} d\theta \right]^2,$$

using Cruz' density of states, this is just

$$C_\ell = \frac{8\pi^2 \nu \kappa^3 \epsilon^2}{3} \int_{\theta_c^{\min}}^{\theta_c^{\max}} \frac{1}{\theta_c^3} d\theta_c \left[\int_0^\pi \frac{\sin \theta P_\ell(\cos \theta)}{\sqrt{1 + 4 \left(\frac{\theta}{\theta_c}\right)^2}} d\theta \right]^2 \quad (23)$$

For numerical integration, we shall also use the Bessel function approximation: use (21) and take the integration limit to ∞ . This is easy to modify for a different

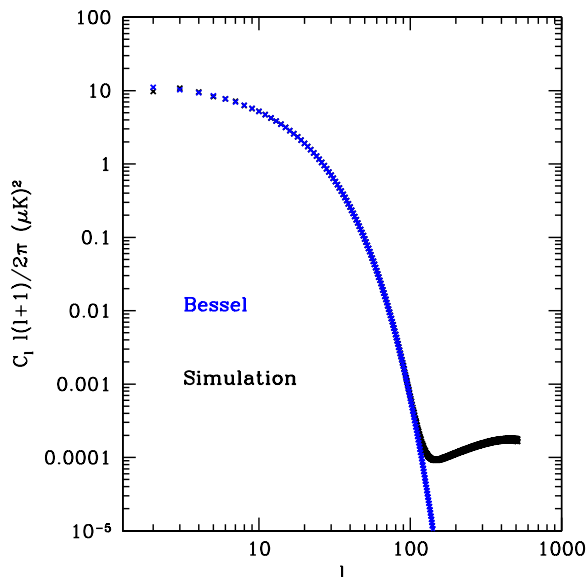


FIG. 7: Texture power spectra; comparing analytic expression & simulation. Uses the exact temperature distortion for a single spot, size $\theta_c = 0.1$ rad. The analytic spectrum uses the Bessel function approximation (22).

distribution, such as that derived; see Fig (8) for the power spectrum using the derived distribution.

2. General Power Spectrum Theory

Let us quickly generalise the power spectrum for a collection of objects.

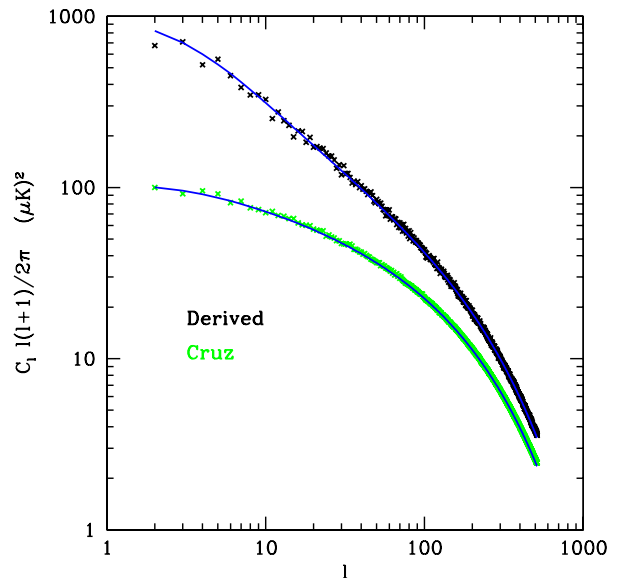


FIG. 8: Texture only power spectra. Numerical analysis of the dependance of the power spectra on distribution. Shown is the derived distributed, and Cruz'; using 20 realisations of the derived power spectrum and 250 realisations of Cruz'. Solid blue lines are the corresponding analytic power spectra. We have used the exact temperature distortion.

Suppose that some function $\zeta(\theta, \phi, \alpha)$ may be expanded into spherical harmonics (i.e. one finds the angular transform). The function is dependent upon coordinate position (θ, ϕ) on the sky, and angular size α of the objects. So that the expansion coefficient is

$$a_{\ell m}(\alpha) = \int d\Omega \zeta(\theta, \phi, \alpha) Y_{\ell m}^*(\theta, \phi),$$

and the power spectrum coefficient

$$C_\ell = \frac{1}{2\ell + 1} \int_{\alpha_{\min}}^{\alpha_{\max}} \left\{ \frac{dn}{d\alpha} \times \sum_m \left| \int d\Omega \zeta(\theta, \phi, \alpha) Y_{\ell m}^*(\theta, \phi) \right|^2 \right\} d\alpha, \quad (24)$$

where we suppose that objects are distributed with $dn/d\alpha$ in some interval $\alpha \rightarrow \alpha + d\alpha$; with fairly obvious upper and lower sizes. We have also used the standard notation for the solid angle element $d\Omega \equiv \sin \theta d\theta d\phi$. This expression has already accounted for positioning of the objects, under a Poissonian distribution. This is an adaptation of the theory discussed in [9].

3. Power Spectra in the Literature

There are power spectra of textures in the literature, such as [10], [11] and [12], however, their spectra differ from ours. It is suspected that their spectra do not

“start” at recombination, as ours do, considering the line ‘We numerically integrate our system of equations from redshift $z = 10^7$ up to the present’ in [11]. They do incorporate an optical depth parameter to take care of this.

In “correct language”, we have computed the power spectrum due to textures, incorporating only the Integrated Sachs-Wolfe (ISW) effect; which is the interaction of photons travelling through a varying gravitational potential, since recombination. What we have not taken into account, is any effect due to textures pre-recombination, or intrinsic textures.

III. COVARIANCE MATRICES

Now, in a similar fashion to quantum mechanics, we can compute the overlap of the C_ℓ 's.

Consider the combination of the power spectrum coefficients

$$D_{\ell\ell'} \equiv \frac{\langle C_\ell C_{\ell'} \rangle - \langle C_\ell \rangle \langle C_{\ell'} \rangle}{\sqrt{\langle C_\ell \rangle \langle C_{\ell'} \rangle}},$$

where averages are taken over N realisations

$$\langle C_\ell \rangle = \frac{1}{N} \sum_{i=1}^N C_\ell^i.$$

So, let us consider $D_{\ell\ell'}$: it shows the overlap between one C_ℓ and all the other $C_{\ell'}$'s. Thus, in a distribution which is completely independent (i.e. a Gaussian distribution), we would expect $D_{\ell\ell'}$ to be diagonal. Infact, the quantity is the variance $\sigma_{C_\ell}^2$, for the diagonal case. Thus, the entire matrix $D_{\ell\ell'}$ is the variance overlap matrix. If we compute the quantity

$$\Sigma_{\ell\ell'} \equiv \sqrt{D_{\ell\ell'} \left(\frac{2\ell+1}{2} \frac{2\ell'+1}{2} \right)^{1/2}}, \quad (25)$$

then it will give us the normalised, symmetric, variance overlap matrix. Such a matrix is called a “covariance matrix”.

Now, consider another type of covariance matrix. Instead of computing for C_ℓ 's, let us compute the overlap of the $a_{\ell m}$'s. Now, to do so, we shall introduce an index ‘ s ’ that will uniquely define a combination of ℓ and m

$$s \equiv \ell(\ell+1) + m, \quad (26)$$

so that we can make the unique identification

$$a_s = a_{\ell m}.$$

We have that the number of s 's, for a given ℓ_{max} is

$$s_{max} = (\ell_{max} + 1)^2 - 1.$$

So then, the covariance matrix we compute here is

$$A_{ss'} \equiv \sqrt{\frac{\ell(\ell+1)}{2\pi} \frac{\ell'(\ell'+1)}{2\pi}} \langle a_s a_{s'}^* \rangle.$$

The diagonal elements of this is the quantity one plots in a power spectrum.

So then, we are able to plot two types of covariance matrix. $\Sigma_{\ell\ell'}$ is the normalised power spectrum variance matrix; which shows correlation between C_ℓ and $C_{\ell'}$; and $A_{ss'}$ the correlation between $a_{\ell m}$ and $a_{\ell' m'}$.

Computing for CMB anisotropies reveals that both matrices are diagonal, thus that anisotropies are Gaussian distributes. We now repeat this for our texture only sky. A procedure like this will highlight dependancies of a peak on those around it. That is, over a large number of realisations, any off-diagonal peaks will be due to the inter-dependancy of C_ℓ with $C_{\ell'}$.

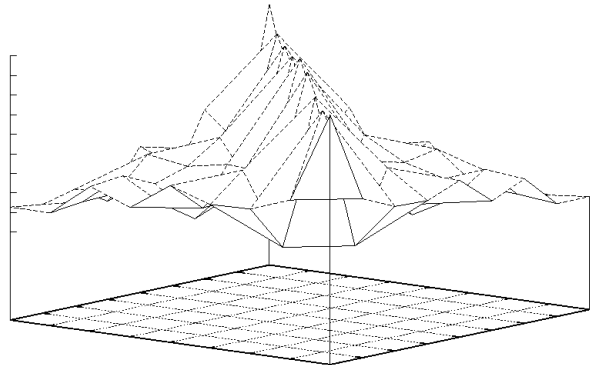


FIG. 9: The covariance matrix $\Sigma_{\ell\ell'}$ for the texture only sky. This is for $\ell_{max} = 10$ and 200 realisations. We have tilted the view like this to highlight the non-diagonal nature of the matrix, in comparison with the CMB anisotropy case.

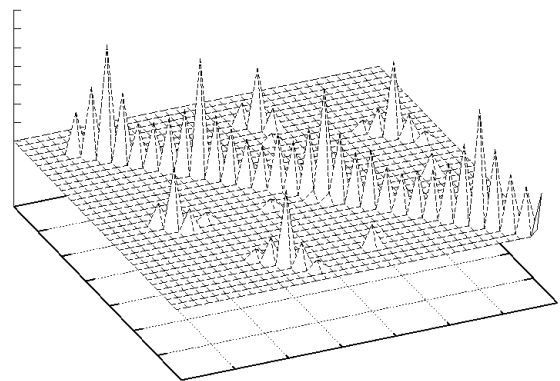


FIG. 10: The covariance matrix $A_{ss'}$ for 200 realisations of the texture only sky. We have shown maximum decomposition mode $\ell_{max} = 5$. On the two horizontal axes we have s, s' . The vertical axis is the value of $A_{ss'}$. We have removed the “noise” from the matrix, by ignoring anything below 20% of the first peak on the left. Notice the modulation of the diagonal peaks; this is not present in the CMB-only case.

If a small amount of analysis of Fig (10) is done; such as finding the off-diagonal values of (ℓ, m) and (ℓ', m') cor-

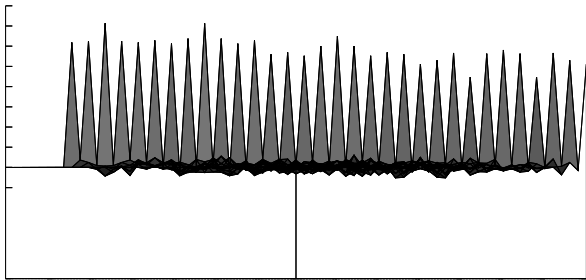


FIG. 11: The covariance matrix $A_{ss'}$ for 500 realisations of the texture and CMB sky. We have shown maximum decomposition mode $\ell_{max} = 5$. On the two horizontal axes we have s, s' . The vertical axis is the value of $A_{ss'}$. This edge-on view shows some modulation of the diagonal elements (off-diagonals have very low amplitude, possibly only due to noise), which is an effect of the textures on the CMB.

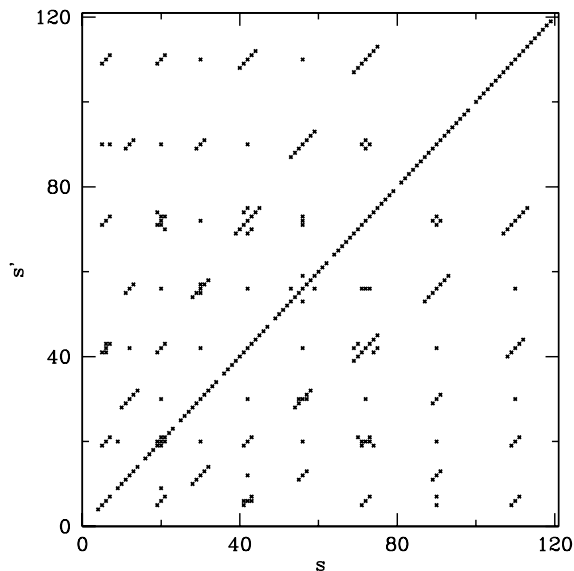


FIG. 12: The positions of the non-zero entries of the covariance matrix $A_{ss'}$ for the texture only sky; after the 20% noise subtraction (i.e. $A_{ss'} > 8.4(\mu\text{K})^2$). This is extended to $\ell_{max} = 10$, still having 200 realisations.

responding to $A_{ss'} > 40(\mu\text{K})^2$, one finds some rather curious correspondences; such as an even-even and odd-odd correspondence to off-diagonal peaks. We see a marked

difference in this and the anisotropy covariance matrix, in that this is not diagonal. The large peaks along the diagonal correspond to where $m = 0$, implying some preferential axial symmetry for the system of textures.

We find that all such off-diagonal values of $A_{ss'}$ have $m = m' = 0$, and an even ℓ corresponds to an even ℓ' ; and odd ℓ to odd ℓ' .

IV. BISPECTRUM

Now, when we said that C_ℓ is the power spectrum coefficient, we neglected to say that it was the two-point angular correlation function. That is, it displays information on the dependance of one angular size with another. We can thus go on to define a three-point correlation function. We follow [13] in definitions used.

Let us start by stating a definition

$$B_{\ell_1 \ell_2 \ell_3}^{m_1 m_2 m_3} \equiv a_{\ell_1 m_1} a_{\ell_2 m_2} a_{\ell_3 m_3}.$$

Now this notation we will compress into

$$B_{\{\ell_i\}}^{\{m_i\}} \equiv \prod_i \{a_{\ell_i m_i}\}; \{\ell_i\}, \{m_i\} \equiv (\ell_1, \ell_2, \ell_3), (m_1, m_2, m_3).$$

So then, from this, we can form a quantity only in $\{\ell_i\}$

$$B_{\{\ell_i\}} = \sum_{\{m_i\}} \begin{pmatrix} \ell_1 & \ell_2 & \ell_3 \\ m_1 & m_2 & m_3 \end{pmatrix} B_{\{\ell_i\}}^{\{m_i\}},$$

and we then define a normalised quantity

$$I_{\{\ell_i\}}^3 \equiv \alpha_{\{\ell_i\}} \frac{B_{\{\ell_i\}}}{(\{C_{\ell_i}\})^{1/2}}, \quad (27)$$

where we have defined

$$\alpha_{\{\ell_i\}} \equiv \frac{1}{[\prod_i (2\ell_i + 1)]^{1/2}} \begin{pmatrix} \ell_1 & \ell_2 & \ell_3 \\ 0 & 0 & 0 \end{pmatrix}^{-1};$$

where we have made use of the Wigner-3J symbol

$$\begin{pmatrix} \ell_1 & \ell_2 & \ell_3 \\ m_1 & m_2 & m_3 \end{pmatrix} \equiv \frac{(-1)^{\ell_1 - \ell_2 - m_3}}{\sqrt{2\ell_3 + 1}} \langle \ell_1 m_1 \ell_2 m_2 | \ell_3 - m_3 \rangle.$$

Where a 3J symbol is the 3-state analogue of the Clebsch-Gordan coefficients in quantum mechanics; the CB coefficients give information on the overlap between two states. In general, we replace the ' ℓ ' above with ' j ', but for our purpose, ℓ is sufficient.

So then, we may choose various combinations of $\{\ell_i\}$ in (27). Supposing we chose

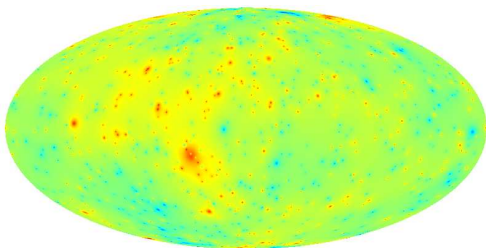
$$\ell_1 = \ell - 2, \quad \ell_2 = \ell, \quad \ell_3 = \ell + 2,$$

then, the quantity we get we further define to be J_ℓ^3 , and is a quantity with a single index. J_ℓ will describe the dependance on the angular size ℓ of an object, with those at $\ell \pm 2$ around that object.

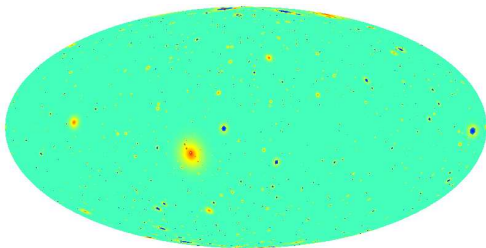
So, for a Gaussian distribution, all J_ℓ will be zero: nothing is dependent on anything else. Infact, we see this with the two-point correlation plots in the covariance matrix $\Sigma_{\ell\ell'}$. However, for a distribution of texture, we have seen that it is not Gaussian, and may produce an “interesting” set of J_ℓ . Infact, a non-Gaussian distribution may still have zero bispectrum, which we see from our plots.

Just as plotting ℓ against C_ℓ (or a combination thereof) constituted plotting a power spectrum, we say that plotting ℓ against J_ℓ is the *bispectrum*. Plotting the bispectrum reveals points dotted about zero, thus we say that a texture distribution has no bispectrum.

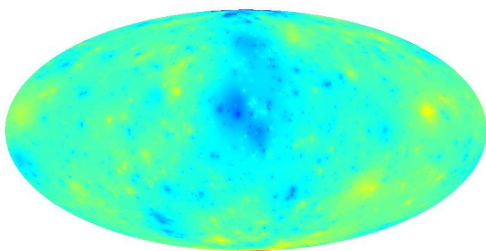
V. SKY MAPS



(a)Exact distortion & Cruz' distribution.



(b)Cruz' distribution & Gaussian half-max temperature distortion.



(c)Exact temperature distortion & derived distribution.

FIG. 13: Texture only skies

VI. DISCUSSION & CONCLUSIONS

Here we shall present our main results, with neither the algebraic derivation or graphical representation of previous sections.

We have simulated skies being solely populated with texture; which are an unstable form of topological defect. The observed size θ_c of a spot is purely due to the redshift z it unwound at;

$$\theta_c = \frac{2\sqrt{2}\kappa(1+z)}{E(z) \int_0^z \frac{dz'}{E(z')}} , \quad E(z) \equiv \sqrt{\Omega_m(1+z)^3 + \Omega_\Lambda}.$$

We may then populate a sky with textures of a range of sizes, where the number of a particular size conforms to some distribution function, which we derive to be

$$\frac{dN}{d\theta_c} = 8\pi\nu \left(\frac{\kappa^3}{3\theta_c^3} + \frac{7\kappa^2}{2\theta_c^2} \right), \quad (28)$$

where we have neglected a non-contributory logarithmic term. Cruz uses an approximation to this, by further neglecting the $\frac{1}{\theta_c^2}$ term above. We find that Cruz' approximation is not well motivated by numerical analysis.

Further to a distribution function, we also have the temperature distortion, at distance ϑ from the centre of a spot, of size θ_c ;

$$\frac{\Delta T}{T}(\vartheta) = \pm \frac{\epsilon}{\sqrt{1 + 4 \left(\frac{\vartheta}{\theta_c} \right)^2}}.$$

To remedy this distortions logarithmic decay, we derived the Gaussian fit $g(\theta) = Ae^{-\theta^2/2\sigma^2}$ to this temperature distortion, once the distance from the spot is sufficient for the distortion to be $1/n^{\text{th}}$ of the value at the spots centre; that is, corresponding to

$$\vartheta \geq \frac{\theta_c}{2} \sqrt{n^2 - 1},$$

and that the amplitude and mean of the Gaussian are

$$A = \frac{\epsilon}{n} e^{(n^2-1)/(2n^2)}, \quad \sigma = \frac{n\theta_c}{2}.$$

Using a Gaussian fit to the temperature distortion has the effect of “cutting off” the distortion, leaving subsequent sky maps looking a little stunted; the “stunted-ness” of the map is proportional to n ; with higher n leaving a more natural looking map.

Thus, given the temperature distortion & distribution of texture spots, we simulated a sky, and decomposed into spherical harmonics. This then allows a power spectrum to be drawn, covariance matrices computed & bispectrum plotted.

We find that the amplitude of the texture power spectrum is of the order $100(\mu\text{K})^2$, in comparison with the CMB anisotropy power spectrum having amplitude of

the order $3000(\mu\text{K})^2$. From the power spectrum, we are able to check for the Gaussian distributed nature of textures; we find that textures are non-Gaussian distributed, in contrast to the CMB anisotropies being Gaussian distributed. Upon plotting the bispectrum (i.e. three-point correlation) of the texture sky, we find that there is no deviation from the CMB anisotropies bispectrum. This does not conclude that textures are Gaussian distributed, more that textures are distributed in a non-Gaussian way, retaining a zero bispectrum.

Following the decomposition of a texture sky, we compute the covariance of decomposition coefficients; into a covariance matrix. We find that off-diagonal elements are present, with even-even and odd-odd mode correspondence. There is also a preference for axial symmetry along the diagonal, with some modulation. This is in contrast to the CMB anisotropies matrix, which is completely diagonal, and all diagonal elements having the same amplitude. Again, that the matrix is non-diagonal points towards the non-Gaussian nature of the texture distribution.

Following the simulated work, we then attempt to compute the power spectrum analytically. Using the standard procedure for decomposition of a function into a basis, we are able to derive that

$$C_\ell = \pi\epsilon^2 \int_{\theta_c^{\min}}^{\theta_c^{\max}} \frac{dN}{d\theta_c} \left[\int_0^\pi \frac{\sin\theta P_\ell(\cos\theta)}{\sqrt{1+4\left(\frac{\theta}{\theta_c}\right)^2}} \right]^2,$$

is the power spectrum coefficient for a sky filled with textures, conforming to some distribution $dN/d\theta_c$. We have

approximated the Legendre polynomial $P_\ell(\cos\theta)$ by a zeroth order Bessel function, of the first kind, for computational ease.

That the textures are non-Gaussian provides a way in which they could be detected, within a background of Gaussian distributed. That is, providing no other non-Gaussian sources, detected non-Gaussianity may then be attributed to texture.

In deriving the analytic power spectrum of textures, we have created a method for finding such spectra, in computational time of the order minutes, as opposed to hours from (proper) simulations. Previous spectra have been computed from vast spatial simulations, where textures unwind according to some evolution equation; and this is the procedure we have “worked around”. All results here, given a correct temperature distortion function, and distribution, are correct, up to the ISW effect, and not intrinsic.

Unresolved Issues: We have left some points open, or not properly discussed. These are the possibility of the temperature distortion function being incorrect (the $1/\theta$ dependence is “bad”), and that the distribution function of Cruz seems to be a very badly motivated approximation.

Acknowledgments

We acknowledge use of the JPL software HEALPix, as well as NASA’s LAMBDA data resource.

I would like to thank my supervisor, R.Battye, for providing time, help & patience throughout this summer project.

-
- [1] M. Cruz, N. Turok, P. Vielva, E. Martinez-Gonzalez, and M. Hobson (2007), astro-ph/07105737.
 - [2] A. Villenkin and E. Shellard, *Cosmic Strings and Other Topological Defects* (Cambridge University Press, 2000).
 - [3] R. Durrer, M. Kunz, and A. Melchiorri, Phys. Rep. **364**, 1 (2002).
 - [4] N. Turok, Phys. Rev. Lett. **63** (1989).
 - [5] N. Guerreiro, P. Avelino, J. Carvalho, and C. Martins (2008), astro-ph/08074373.
 - [6] R. Durrer, Phys. Rev. D. **42** (1990).
 - [7] N. Turok and D. Spergel, Phys. Rev. Lett. **64**, 2736 (1990).
 - [8] H. Press, B. Flannery, S. Teukolsky, and W. Vetterling, *Numerical Recipes* (Cambridge University Press, 1986).
 - [9] S. Cole and N. Kaiser, Mon. Not. R. Astr. Soc. **233**, 637 (1988).
 - [10] U. Pen, U. Seljak, and N.Turok, Phys. Rev. Lett. **79** (1997).
 - [11] R. Durrer, M. Kunz, and A. Melchiorri, Phys. Rev. D. **59**, 123005 (1999).
 - [12] N. Bevis, M.Hindmarsh, and M. Kunz, Phys. Rev. D. **70**, 043508 (2004).
 - [13] N. Phillips and A. Kogut (2000), astro-ph/0010333.